

# Tunability of the superconductivity of tungsten films grown by focused-ion-beam direct writing

Wuxia Li,<sup>\*1</sup> J. C. Fenton<sup>1</sup>, Yiqian Wang<sup>2</sup>, D.W. McComb<sup>2</sup>, and P. A. Warburton<sup>\*1</sup>

<sup>1</sup> London Centre for Nanotechnology, University College London, WC1H 0AH (UK)

\* Email: p.warburton@ee.ucl.ac.uk; w.li@ee.ucl.ac.uk

<sup>2</sup> London Centre for Nanotechnology and Department of Materials  
Imperial College, London, SW7 2AZ (UK)

Copyright 2008 American Institute of Physics. This article may be downloaded for personal use only. Any other use requires prior permission of the author and the American Institute of Physics.

The following article appeared in J. Appl. Phys. 104 093913 (2008) and may be found at <http://dx.doi.org/10.1063/1.3013444>

## Abstract

We have grown tungsten-containing films by focused-ion-beam (FIB)-induced chemical vapor deposition. The films lie close to the metal-insulator transition with an electrical conductivity which changes by less than 5% between room temperature and 7 K. The superconducting transition temperature  $T_c$  of the films can be controlled between 5.0 and 6.2 K by varying the ion-beam deposition current. The  $T_c$  can be correlated with how far the films are from the metal-insulator transition, showing a nonmonotonic dependence, which is well described by the heuristic model of Osofsky et al. (Phys. Rev. Lett. 87, 197004 (2001)). Our results suggest that FIB direct-writing of W composites might be a potential approach to fabricate mask-free superconducting devices as well as to explore the role of reduced dimensionality on superconductivity.

Keywords: Direct-writing, nanoscale structures, superconductivity, tungsten, focused-ion-beam deposition

## Introduction

The investigation of enhanced superconductivity has been a major activity in solid-state physics and materials science in the last few decades. There are only 27 elements which, in bulk form, are superconductors at ambient pressure. The highest critical temperature,  $T_c$ , of an elemental bulk material is that of niobium ( $T_c = 9.3$  K). Thus the search for higher- $T_c$  superconductors was expanded to alloys, compounds and composites.<sup>[1-8]</sup> In an alloy, the degree of order can be very important in determining the superconducting properties. For high transition-temperature superconductors the stoichiometric composition and the structural order are of great importance in obtaining a maximal  $T_c$ . By contrast, highly disordered transition metals mostly display a higher  $T_c$  than their annealed ordered counterparts. Tungsten is the superconductor of choice for fabrication of transition-edge sensors (TESs) for optical and near-infrared wavelengths due to the tunability of its superconducting transition temperature in the range  $\sim 100$  mK and its relatively weak electron-phonon coupling at such temperatures.<sup>[9]</sup> Single-crystal tungsten has a very low transition temperature:  $T_c$  of alpha (bcc) W is 15 mK and that of beta (A15) W is in the range 1 K to 4 K. Amorphous tungsten films<sup>[4-5]</sup> and alloys,<sup>[6-8]</sup> when rendered into a disordered or granular state, have a  $T_c$  which can be up to two orders of magnitude larger than that of single-crystal bcc W.

Recently the use of a focused ion- or electron-beam to induce the deposition of composite materials from metal-organic precursors has emerged as an important nanofabrication technique.<sup>[10-18]</sup> Such techniques enable the formation of metallic

interconnects in a single ‘writing’ step, with a resolution comparable to structures defined by electron-beam lithography. Studies have been performed to explore the growth mechanism,<sup>[11,12]</sup> the transport properties<sup>[10,13,16]</sup> and their application in prototype device fabrication.<sup>[17,18]</sup> Sadki *et al.* first demonstrated that focused-ion-beam (FIB) deposited tungsten was superconducting, obtaining a  $T_c$  of 5.2 K.<sup>[10]</sup> This result was subsequently confirmed by Luxmoore *et al.*<sup>[13]</sup> Both groups qualitatively ascribe the comparatively high  $T_c$  in FIB-deposited tungsten to the absence of long-range order in the crystal structure of the deposited material. However, the mechanism behind the significantly enhanced superconductivity of such materials is not clear. Can the superconductivity of FIB-deposited tungsten be tuned by varying the growth parameters? Can we exploit the three-dimensional fabrication possibilities offered by FIB to make free-standing superconducting nanowires? Understanding the answers to these questions is of both great engineering importance and fundamental research interest.

To address these issues, we have grown tungsten-containing nanowires by FIB-induced chemical vapour deposition. Here we report systematic experiments which confirm in a quantitative fashion that the enhanced  $T_c$  in FIB-deposited metallic tungsten is directly related to how close the deposited material lies to the metal-insulator transition (MIT). Due to the competition between the electronic density of states (which is *reduced* as the MIT is approached) and the electron-phonon interaction (which is *increased* due to an increase in the electron screening length as the MIT is approached) there is a natural maximum in  $T_c$  close to the MIT. We can control the proximity to the MIT by varying the ion-beam deposition current, and hence we have a mechanism for controlling the  $T_c$  of the deposited material during growth. We also report the superconducting properties of free-standing three-dimensional tungsten nanostructures grown using a 1pA ion-beam current. The flying W nanowire is superconducting with a  $T_c$  above 5.1 K and can be repeatedly thermally cycled. Our results suggest a possible method to control the properties of W-containing materials for mask-free superconducting nanoscale device fabrication. Possible device applications include superconducting nanowire single-photon detectors,<sup>[19]</sup> superconducting nanomechanical resonators for studies of macroscopic quantum phenomena<sup>[20]</sup> and compact vertical inductors for high-frequency environmental isolation of superconducting qubits.<sup>[21]</sup>

## Experimental

*Growth of lateral and 3D flying tungsten nanoscale structures:* A commercially available FIB (Carl Zeiss XB1540) system utilizing a beam of 30 keV singly-charged Ga<sup>+</sup> ions was used. Tungsten hexacarbonyl (W(CO)<sub>6</sub>) gas was injected onto the sample surface through a nozzle, creating a local high pressure in the region scanned by the ion beam. The base pressure before introducing the precursor gas was  $2.4 \times 10^{-6}$  mbar. During deposition the system pressure was in the range  $7.4 - 8.3 \times 10^{-6}$  mbar. Before the W deposition, gold contact patterns were formed onto Si substrates with a 200-nm-thick oxidized silicon layer. These patterns were achieved by conventional photolithography-based processes, which include: (i) photolithography to define a pattern on the substrate surface using a Karl Suss MJB3 Mask Aligner. Pattern definition is accomplished by spinning a layer of Shipley S1818 photoresist (an ultraviolet-light-sensitive liquid) onto the substrate surface and baking at 90°C for 2 mins; then selectively exposing the resist to ultraviolet light through a mask. (ii) deposition of a 10-nm-thick Ti layer followed by a 200-nm-thick Au layer on the sample by an Edwards e-beam evaporator. (iii) lift-off to remove the unwanted metal by soaking the sample in acetone. The four-terminal configurations were fabricated by the following steps: first an ion beam with a certain ion-beam current was scanned over an area with a nominal size of 45  $\mu\text{m}$  in length and 0.5  $\mu\text{m}$  in width to deposit tungsten to bridge a pair of gold contact pads (labelled I<sup>+</sup> and I in figure 1(a)), then the voltage contacts were deposited using identical deposition conditions to those used for the nanowire. Various ion-beam currents, 1, 5, 20, 50, 200, 500 and 1000 pA

were used to form four-terminal configurations. A constant ion fluence of  $1.78 \text{ nC}/\mu\text{m}^2$  was applied. The ion beam was scanned with a frequency of 20,000 Hz and 0.02 Hz in the X and Y directions respectively, where the X direction lies along the length of the nanowire and the Y direction is transverse to it. In parallel a series of tungsten strips was deposited using a fixed ion beam current of 20 pA with various ion fluences to examine the thickness-dependence of the superconducting transitions. The width of the nanowires was measured *in-situ* by SEM and the thicknesses were measured by a Dektak 8 Surface Profiler.

For nanoscale 3D flying tungsten structure fabrication, a lateral tungsten strip was first deposited to close the gap between the gold contact pads to around  $1.0 \mu\text{m}$ . After that, the 1 pA ion-beam was scanned for 2 mins in an area of  $80 \text{ nm} \times 80 \text{ nm}$  on the edge of the gold contact pad to form a vertical rod. Next a tilted portion was grown on the top of this vertical rod by shifting the beam electrostatically at a rate of  $3 \text{ nms}^{-1}$  for a total time of 6 mins. Thus one limb of the suspending structure has been formed. To grow the other limb, first the beam was scanned for 6 mins in a  $80 \text{ nm} \times 80 \text{ nm}$  area on the edge of the tungsten strip, then beam-shifting was used to grow a tilted part using the same scan area as for the vertical part.

*Compositional and structural property analyses:* The chemical composition was obtained by energy dispersive X-ray spectroscopy (EDS) with an accelerating voltage of 15 kV. Features with a nominal scan area of  $2.0 \mu\text{m} \times 2.0 \mu\text{m}$  were deposited under the same deposition conditions as for the lateral nanowires. The microstructure was analyzed by FEI TITAN scanning transmission electron microscopy for both lateral nanowires and vertical nanorods grown on holey carbon TEM grids. After growth, the vertical rods were felled onto the carbon grid using very low current FIB- milling through the foot of the rod (the ion beam was at normal incidence to the rod).

*Low-temperature transport properties characterisations:* Current-biased transport measurements were performed with the sample mounted on a “dip-stick” immersed in a liquid-helium storage dewar. The chip under test was first stuck to a copper chip-carrier by silver paste and dried in air, then gold wire bonding was employed to connect the gold contact pads on the chip to copper pads on the chip carrier. The chip carrier was mounted on a copper block at the end of the dip-stick probe. Also attached to this copper block was a Lakeshore Cernox resistance temperature sensor. This sensor was connected to an Oxford Instruments Intelligent Temperature Controller in order to measure the temperature. Transport measurements were performed with a home-made current source and voltage amplifier. All the data acquisition and analysis were controlled by a LabVIEW-based platform.

## Results and discussion

We begin by discussing the compositional and structural properties of the grown nanowires. Four-terminal structures were formed on substrates that consist of 200-nm-thick gold test patterns previously deposited onto oxidized silicon substrates. An ion beam was scanned across the substrate causing local decomposition of  $\text{W}(\text{CO})_6$  gas molecules. Volatile by-products were desorbed from the substrate and pumped away through the vacuum system, whereas the W together with C and O adhered to the surface to form the deposit. Ga from the ion source is also present in the composites. The nominal size of the nanowires was  $45 \mu\text{m}$  in length and  $0.5 \mu\text{m}$  in width. The thickness of the nanowires varied between 120 nm and 250 nm according to the growth conditions. **Fig. 1(a)** shows a typical SEM image of the FIB-deposited four-terminal configuration for temperature-dependent resistivity measurements. Chemical composition analysis was carried out on larger features grown under identical conditions. The atomic concentrations of C, Ga and W as a function of the primary ion-beam current,  $I_p$ , are shown in Fig. 1 (b). It can be seen that the C content decreases with increasing  $I_p$ . Conversely, the Ga content and W content increase with increasing  $I_p$ . This behavior is similar to the composition variation of FIB-deposited Pt.<sup>[14]</sup>

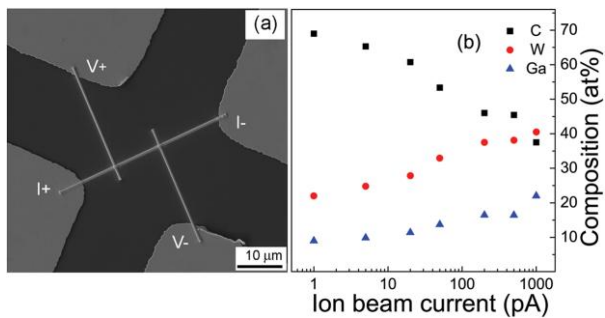


Figure 1. (a) Plan-view SEM image of a four-terminal contact configuration for temperature-dependent resistivity measurements; (b) Atomic concentrations for C, W and Ga in the deposited material as a function of the ion-beam current.

Fig. 2 (a) shows a high-resolution transmission electron microscope (HRTEM) image of a nanowire showing the absence of long-range crystalline order. Inspection of the image at a higher magnification (Fig. 2 (b)) shows the possible presence of nanocrystallite clusters with size of order of 1 nm. We found no noticeable variation in the HRTEM images with ion-beam deposition current. In addition nanowires which were grown vertically (*i.e.* perpendicular to the substrate surface) showed similar nanostructure as shown by HRTEM to those grown horizontally (*i.e.* parallel to the substrate surface.).

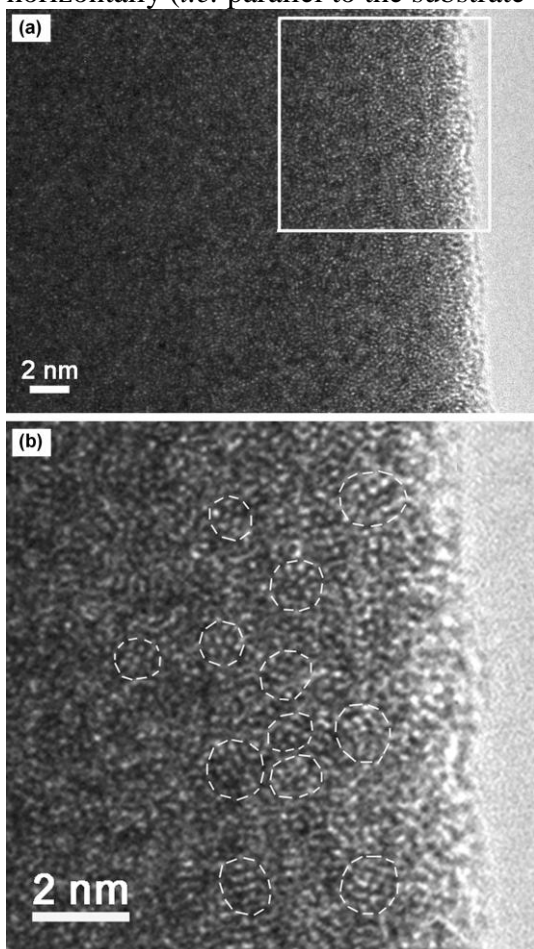


Figure 2. (a) HRTEM image of a nanowire showing the edge of the wire; (b) HRTEM image of a selected area (as indicated by the square in Fig.2 (a)) at a higher magnification. Short-range ordered microstructure is visible (refer to dotted circles).

We conclude that our FIB-deposited “tungsten” is very different from crystalline tungsten both in terms of its compositional content and its structure. It is possible, however, that the nanometre-sized regions of short-range structural order could have an effect on the electrical transport properties of the nanowires. Luxmoore *et al.*<sup>[13]</sup> formed material by electron-beam induced deposition using the same precursor and found an amorphous-like microstructure showing no superconducting transition down to 1.6 K. This further indicates the importance of the degree of order in the enhancement of superconductivity of FIB deposited W.

We now discuss our electrical transport measurements. A constant current of 1.0  $\mu\text{A}$  was applied to the two outer terminals and the voltage was measured between the other two terminals as shown in Fig. 1 (a). The temperature dependence of the resistivity is shown in Fig. 3 (a) for several nanowires grown with  $I_p$  ranging from 1 pA to 1 nA. In the normal state the resistivity is very weakly temperature-dependent from just above the superconducting transition all the way up to room temperature (with an electrical conductivity which changes by less than 5% between room temperature and 7 K), suggesting that the material is very close to the MIT. All the wires show superconducting transitions above 5.0 K; fig 3(b) shows a typical example of the transition for one nanowire. In Fig. 3 (c) we plot the superconducting transition temperature,  $T_c$ , as a function of the ion-beam deposition current,  $I_p$ . Here  $T_c$  is defined as the temperature at which the resistivity falls to 50% of its value at the onset of the transition.  $T_c$  initially increases with  $I_p$ , reaching a maximum of 6.2 K for wires deposited at 50 pA, and then decreases as  $I_p$  is increased further.

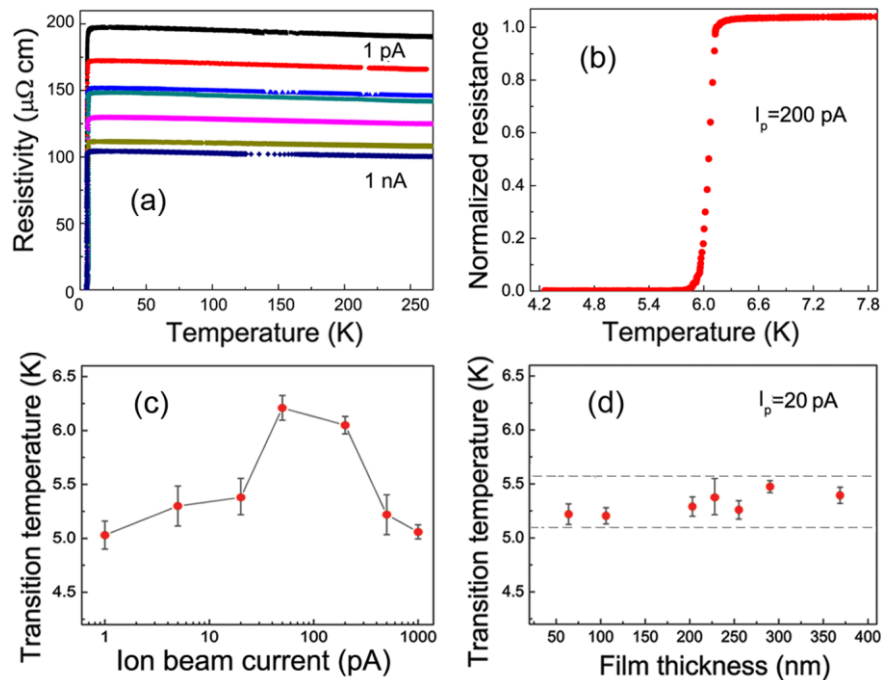


Figure. 3 (a) Resistivity vs. temperature for nanowires deposited with 1 pA (top), 5, 20, 50, 200, 500 and 1000 pA (top) ion beam currents; (b) A representative low-temperature region. The resistivity is normalized to its value at 300 K; (c) Superconducting transition temperature as a function of ion beam current. The line is a guide to the eye. (d) Film-thickness dependence of  $T_c$  for strips grown with 20 pA ion-beam current. In both (c) and (d) the error bars correspond to the transition width ( $\Delta T_c$ ), between temperatures showing 10% and 90% of the resistance at the onset of superconductivity.

The error bars in Fig. 3(b) correspond to the width of the superconducting transition. It can be seen that, with the exception of the nanowire grown at 1 nA, samples with higher  $T_c$

have sharper transitions, suggesting a correlation between the  $T_c$  and the *intra*-sample structural and/or compositional homogeneity. Nevertheless, the fact that the *foot* of the superconducting transition for nanowires with higher  $T_c$  occurs at a significantly higher temperature than the *onset* of the transition for nanowires with lower  $T_c$  shows that variations in *intra*-sample inhomogeneity alone cannot account for the *inter*-sample  $T_c$  variation.

In order to rule out film thickness variation as a possible source of the  $T_c$  variation in our nanowires we deposited seven nanowires with different thicknesses (between 60 nm and 370 nm) at a fixed ion-beam deposition current. Figure 3(d) shows the thickness dependence of the  $T_c$  of these nanowires. All these nanowires have a  $T_c$  around 5.3 K, with a standard deviation of 0.13 K. Thus we believe that the thickness variation of nanowires grown at different deposition currents does not play a significant role in the  $T_c$  variation. Figure 4 (a) shows the dependence of  $T_c$  on W content. The dependence is non-monotonic, as is the dependence upon C and Ga content (not shown). This rules out the possibility that the material is an alloy superconductor with a  $T_c$  simply given by the weighted average of the  $T_c$ 's of the components of the alloy.<sup>[22]</sup>

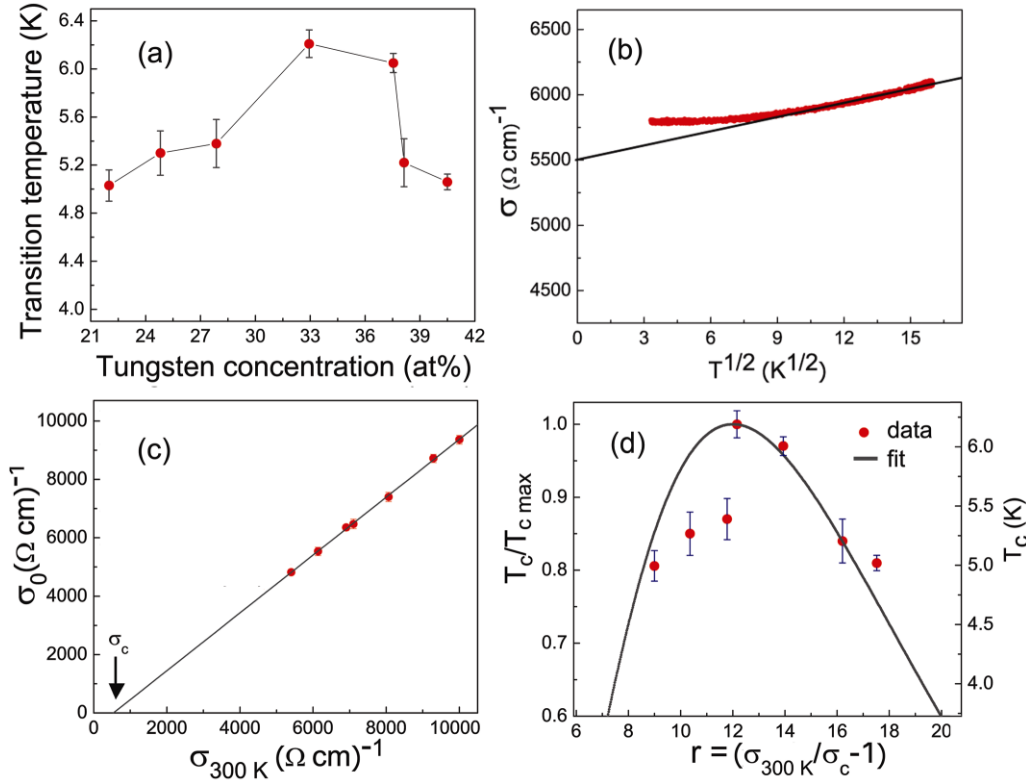


Figure 4 (a) Superconducting transition temperature as a function of W concentration of the nanowires; (b) Representative measurement of the conductivity as a function of  $T^{1/2}$  for the nanowire deposited with a 5 pA ion-beam current. The line is a fit to the high-temperature region illustrating the method used to extract the zero-temperature conductivity,  $\sigma_0$ . (c)  $\sigma_0$  vs the room-temperature conductivity,  $\sigma_{300 \text{ K}}$ . The line is a fit to the experimental data and is used to derive the sample-independent  $\sigma_c$ ; (d)  $r$  ( $\equiv \sigma_{300 \text{ K}}/\sigma_c - 1$ ) dependence of  $T_c/T_{c \text{ max}}$ ; the curve is a fit to the data using Eq.(1).

Although, as described above, we were not able to discern any inter-sample differences in the nanostructural order of the tungsten as revealed by HRTEM, there is clearly a strong variation in the normal-state conductivity in the samples as shown in figure 3 (a). Since the electronic conductivity of any material is a highly-sensitive function of defect scattering, we

will now therefore use the normal-state conductivity as a *quantitative* measure of the nanostructural order in our tungsten wires and correlate it with the  $T_c$ .

The origin of enhanced superconductivity in disordered metallic systems has been discussed in detail by Osofsky *et al.*<sup>[8]</sup> The physical basis of their model is that disorder enhances the electron screening length over the Thomas-Fermi value for a well-ordered metal. This enhances the BCS interaction potential,  $V$ , which in turn enhances  $T_c$  according to the BCS expression  $T_c \sim \exp(-1/NV)$ . Here  $N$  is the electronic density of states which, by contrast, is *reduced* by disorder. The competition between  $N$  and  $V$  naturally leads to a maximum in  $T_c$  at some value of disorder near to and on the metallic side of the MIT. In the heuristic theory of Osofsky *et al.*,  $T_c$  varies as a function of the parameter  $r \equiv (\sigma_{300K} / \sigma_c) - 1$ . Here  $\sigma_{300K}$  is the room-temperature conductivity and  $\sigma_c$  is the critical conductivity at the MIT. Osofsky *et al.* showed that the theory fits experimental data rather well for a wide variety of disordered metallic alloys, with the maximum  $T_c$  occurring at  $r = 12 \pm 1$ .

In order to extract the critical conductivity,  $\sigma_c$ , for our FIB-deposited tungsten material we directly follow the approach detailed in Ref. 5, to which the reader is referred for full details. We begin by determining the sample-dependent zero-temperature conductivity,  $\sigma_0$ . This is achieved by linearly extrapolating plots of  $\sigma(T^{1/2})$  to  $T = 0$ , as shown in Fig. 4 (b). These values are then plotted as a function of the room-temperature conductivity,  $\sigma_{300K}$ , as shown in figure 4(c). Our data clearly show a linear relationship between  $\sigma_0$  and  $\sigma_{300K}$ . From this we conclude that the (sample-dependent) normal-state electronic properties are determined by the (sample-independent) critical conductivity at the MIT, confirming the role of disorder for  $T > T_c$ . In order to extract this critical conductivity, which is a fundamental material property of FIB-grown tungsten, we take the value of  $\sigma_{300K}$  extrapolated to  $\sigma_0 = 0$  as shown in figure 4(c). This now allows us to calculate the parameter  $r$  which describes how metallic the sample is;  $r = 0$  corresponds to the MIT and increasing  $r$  corresponds to increasing metallicity. In Fig. 4 (d), we plot the dependence of  $T_c$  upon  $r$ .

We now compare our experimental data with equation (6) in Ref. 5. We make the simplifying approximations detailed in Ref. 8 (*viz.*  $\delta = 1, m = 0$ ) with the result that the model predicts

$$\frac{T_c}{T_{C \max}} = \exp \left[ -A \left( r + \frac{r_{\max}^2}{r} - 2r_{\max} \right) \right] \quad (1)$$

Here  $r_{\max}$  is the value of  $r$  at which the maximum  $T_c$  occurs. We set  $r_{\max} = 12$ , consistent with the experiments on MoSi,<sup>[23]</sup> WSi,<sup>[6,8]</sup> WGe<sup>[6]</sup> and SiAu<sup>[24,25]</sup> reported in Ref. 5. The best fit to our data is shown in Fig. 4 (d). The fit supports our conclusion that the  $T_c$  of the tungsten nanowires is determined by the degree of order in the deposited material and specifically by how far from the MIT the material lies.  $A$  is the single fitting parameter and gives an inverse measure of the phonon-mediated electron-electron interaction strength,  $NV$ . Specifically  $NV = (77.5 A)^{-1}$ , which from the fit to our data is equal to  $0.08 \pm 0.01$ . This suggests that FIB-deposited tungsten is a disordered BCS superconductor with relatively weak coupling. For comparison, values of  $NV$  for other tungsten-containing disordered alloys in Ref. 5 are  $0.08 \pm 0.01$  for WGe and  $0.08 \pm 0.02$  or  $0.24 \pm 0.01$  for WSi grown by two different research groups.

Next we discuss the superconducting properties of free-standing 3D tungsten nanostructures grown by a 1 pA ion-beam current. Fig. 5 (a) shows an SEM image of a vertical air-bridge linking two larger contacts; the larger contact at the left is gold and the narrow contact at the right is FIB-deposited tungsten. The wire has a vertical section with diameter below 120 nm, and a sloping section with a smaller diameter. The slope of the sloping section is controllable to a certain extent up to a maximum of 19 degrees.<sup>[8]</sup> Fig. 5 (b) shows the resistive transition measured in a two-terminal configuration. The structure can be repeatedly thermally cycled (while applying a constant current of 1.0  $\mu$ A) without observable

structural deformation or degradation of  $T_c$ . The midpoint of the transition is at 5.3 K and there is a finite low-resistance tail below 5.2 K. We surmise that the former is due to the onset of superconductivity in the horizontal tungsten contact while the latter is the superconducting transition of the vertical structure. In order to remove the ambiguity associated with a two-terminal measurement we also performed a four-terminal measurement on a vertically-grown tungsten nanowire. The four wires were attached after the vertical wire had been felled by FIB-milling through its base. The observation of a similar transition temperature for this felled vertical nanorod (measured in a four-terminal configuration) to that of the 3D air-bridge structure (albeit measured in a two-terminal configuration) confirms that vertically-grown tungsten nanowires have technologically-useful transition temperatures above 4.2 K.

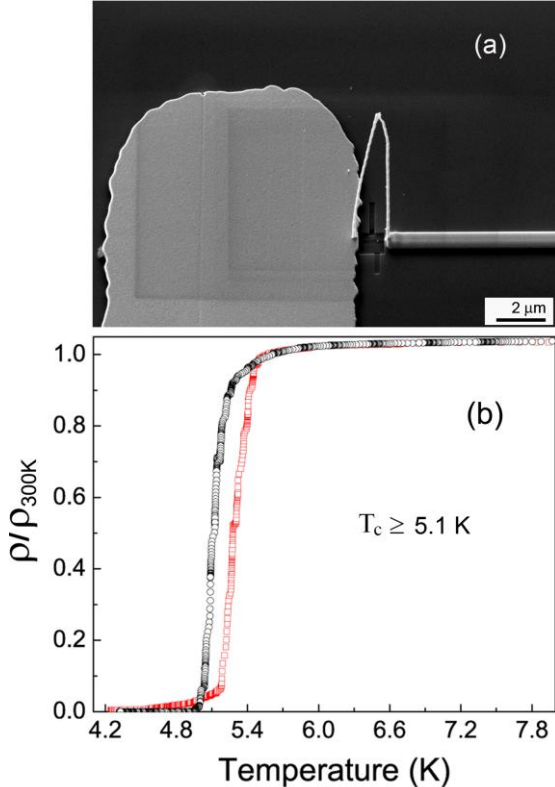


Figure 5. (a) SEM image ( $54^\circ$  viewing angle) of a flying tungsten nanostructure grown by focused-ion-beam deposition using a 1 pA ion beam current; (b) the temperature dependence of the normalised resistivity of the structure shown in (a) (red circles, two-terminal configuration) and that of a felled vertically grown nanorod (black circles, four-terminal configuration).

## Conclusions

In conclusion, we have observed considerable enhancement of  $T_c$  for W nanowires grown by FIB. The  $T_c$  can be controlled between 5.0 K and 6.2 K by varying the ion-beam current. The normal-state conductivity of the wires, which also varies from sample to sample, is determined by the critical conductivity at the metal-insulator transition, this being a sample-independent material property. There is a maximum in the  $T_c$  enhancement close to  $r = 12$  and the results are in good agreement with the model of Osofsky *et al.*<sup>[8]</sup> This confirms the importance of the role of the metal-insulator transition in determining the superconducting properties of disordered metals. Furthermore, 3D flying nanofeatures grown using very low ion-beam current are also superconducting.

We have grown both lateral and flying tungsten nanostructures with reasonably good conductivity and much enhanced superconductivity by focused-ion-beam induced chemical

vapor deposition. These results suggest that FIB direct-writing of W composites might be a useful approach for a number of applications including: (i) fabrication of vertical nanodevices, *e.g.* as electrodes for contacting to the vertical leg of ZnO and CdS tetrapod nanocrystals;<sup>[17]</sup> (ii) mask-free superconducting devices, *e.g.* inductors, nano superconducting quantum interference device (nanoSQUIDs) and superconducting single photon detectors (SSPD); (iii) free-standing nanomechanical resonators for experiments in macroscopic quantum phenomena and qubits. Furthermore, since in principle it is possible to grow tungsten nanowires of diameter as small as a few nm using this method, we believe that this technique will become an important tool in experimental studies of the role of reduced dimensionality on superconductivity.<sup>[26]</sup>

### Acknowledgements

The authors acknowledge Kevin Lee for technical assistance. This work is supported by the IRC in Nanotechnology and by EPSRC contract EP/F035411/1.

### References

- [1] T.G. Berlincourt, R.R. Hake, *Phys. Rev.* **1963**, *131*, 140.
- [2] W. L. Bond, A. S. Cooper, K. Andres, G. W. Hull, T. H. Geballe, B. T. Matthias, *Appl. Phys. Lett.* **1965**, *15*, 260.
- [3] R.A. Hein, J.W. Gibson, and R.D. Blaugher, *Rev. Mod. Phys.* **1964**, *36*, 149.
- [4] S. Basavaiah, S. R. Pollack, *J. Appl. Phys.* **1968**, *39*, 5548.
- [5] M. M. Collver, R. H. Hammond, *Phys. Rev. Lett.* **1973**, *30*, 92.
- [6] S. Kondo, *J. Mater. Res.* **1992**, *7*, 853.
- [7] R. H. Willens, E. Buehler, *Appl. Phys. Lett.* **1965**, *7*, 25.
- [8] M. S. Osofsky, R. J. Soulen, Jr., J. H. Claassen, G. Trotter, H. Kim, J. S. Horwitz, *Phys. Rev. Lett.* **2001**, *87*, 197004.
- [9] D. Rosenberg, A. E. Lita, A. J. Miller, S. W. Nam, *Phys. Rev. A*, **2005**, *71*, 061803.
- [10] E. S. Sadki, S. Ooi, K. Hirata, *Appl. Phys. Lett.* **2004**, *85*, 6206.
- [11] H. Langfischer, B. Basnar, H. Hutter, E. Bertagnolli, *J. Vac. Sci. Technol. A* **2002**, *20*, 1408.
- [12] W. Li, P. A. Warburton, *Nanotechnology* **2007**, *18*, 485305.
- [13] I. J. Luxmoore, I. M. Ross, A. G. Gullis, P. W. Fry, J. Orr, P. D. Buckle, J. H. Jefferson, *Thin Solid Films* **2007**, *515*, 6791.
- [14] K. A. Telari, B. R. Rogers, H. Fang, L. Shen, R. A. Weller, D. N. Braski, *J. Vac. Sci. Technol. B* **2002**, *20*, 590.
- [15] P. Beecher, G. De Marzi, A. J. Quinn, G. Redmond, E. V. Shevchenko, H. Weller, *Appl. Phys. Lett.* **2004**, *85*, 5706.
- [16] E. Horváth P. L. Neumann, A. L. Tóth, Z. E. Horváth, L. P. Biró, *Microelectronic Engineering*, **2007**, *84*, 837.
- [17] M. C. Newton, S. Firth, P. A. Warburton, *Appl. Phys. Lett.* **2005**, *89*, 072194.
- [18] W. Li, T. H. Shen, *Appl. Phys. Lett.* **2005**, *87*, 123113.
- [19] G. N. Gol'tsman, O. Okunev, G. Chulkova, A. Lipatov, A. Semenov, K. Smirnov, B. Voronov, A. Dzardanov, C. Williams, R. Sobolewski, *Appl. Phys. Lett.* **2001**, *79*, 705.
- [20] A. N. Cleland, M. R. Geller, *Phys. Rev. Lett.* **2004**, *93*, 070501.
- [21] A. J. Berkley, H. Xu, M. A. Gubrud, R. C. Ramos, J. R. Anderson, C. J. Lobb, F. C. Wellstood, *IEEE Trans. Appl. Supercond.* **2003**, *13* 952.
- [22] T. Claeson, H. L. Luo, *J. Phys. Chem. Solids* **1966**, *27*, 1081.
- [23] S. Kudo, *J. Appl. Phys.* **1988**, *63*, 2033.
- [24] N. Nishida, M. Yamaguchi, T. Furubayashi, K. Morigaki, H. Ishimoto, K. Ono, *Solid State Commun.* **1982**, *44*, 305.
- [25] T. Furubayashi, N. Nishida, M. Yamaguchi, K. Morigaki, H. Ishimoto, *Solid State*

Commun. **1985**, 55, 305.

[26] A. Bezryadin, C. N. Lau, M. Tinkham, Nature, **2000**, 404 971.